Assessment of NASA GISS CMIP5 and Post-CMIP5 Simulated Clouds and TOA Radiation Budgets Using Satellite Observations. Part I: Cloud Fraction and Properties

RYAN E. STANFIELD, XIQUAN DONG, BAIKE XI, AND AARON KENNEDY

Department of Atmospheric Sciences, University of North Dakota, Grand Forks, North Dakota

ANTHONY D. DEL GENIO

NASA Goddard Institute for Space Studies, New York, New York

PATRICK MINNIS

NASA Langley Research Center, Hampton, Virginia

JONATHAN H. JIANG

Jet Propulsion Laboratory, California Institute of Technology, Pasadena, California

(Manuscript received 15 September 2013, in final form 16 February 2014)

ABSTRACT

Although many improvements have been made in phase 5 of the Coupled Model Intercomparison Project (CMIP5), clouds remain a significant source of uncertainty in general circulation models (GCMs) because their structural and optical properties are strongly dependent upon interactions between aerosol/cloud microphysics and dynamics that are unresolved in such models. Recent changes to the planetary boundary layer (PBL) turbulence and moist convection parameterizations in the NASA GISS Model E2 atmospheric GCM (post-CMIP5, hereafter P5) have improved cloud simulations significantly compared to its CMIP5 (hereafter C5) predecessor. A study has been performed to evaluate these changes between the P5 and C5 versions of the GCM, both of which used prescribed sea surface temperatures. P5 and C5 simulated cloud fraction (CF), liquid water path (LWP), ice water path (IWP), cloud water path (CWP), precipitable water vapor (PWV), and relative humidity (RH) have been compared to multiple satellite observations including the Clouds and the Earth's Radiant Energy System–Moderate Resolution Imaging Spectroradiometer (CERES-MODIS, hereafter CM), *CloudSat–Cloud–Aerosol Lidar and Infrared Pathfinder Satellite Observations* (*CALIPSO*; hereafter CC), Atmospheric Infrared Sounder (AIRS), and Advanced Microwave Scanning Radiometer for Earth Observing System (AMSR-E). Although some improvements are observed in the P5 simulation on a global scale, large improvements have been found over the southern midlatitudes (SMLs), where correlations increased and both bias and root-mean-square error (RMSE) significantly decreased, in relation to the previous C5 simulation, when compared to observations. Changes to the PBL scheme have resulted in improved total column CFs, particularly over the SMLs where marine boundary layer (MBL) CFs have increased by nearly 20% relative to the previous C5 simulation. Globally, the P5 simulated CWPs are 25 g m^{-2} lower than the previous C5 results. The P5 version of the GCM simulates PWV and RH higher than its C5 counterpart and agrees well with the AMSR-E and AIRS observations. The moister atmospheric conditions simulated by P5 are consistent with the CF comparison and provide a strong support for the increase in MBL clouds over the SMLs. Over the tropics, the P5 version of the GCM simulated total column CFs and CWPs are slightly lower than the previous C5 results, primarily as a result of the shallower tropical boundary layer in P5 relative to C5 in regions outside the marine stratocumulus decks.

1. Introduction

The treatment of clouds in climate models and their associated feedbacks have long been one of the largest sources of uncertainty in predicting any potential future

Corresponding author address: Dr. Xiquan Dong, Department of Atmospheric Sciences, University of North Dakota, 4149 University Ave., Stop 9006, Grand Forks, ND 58203-9006.
E-mail: dong@aero.und.edu

DOI: 10.1175/JCLI-D-13-00558.1

climate change (Cess et al. 1989; Wielicki et al. 1995; Houghton et al. 2001; Stephens 2005; Bony et al. 2006; Randall et al. 2007). Zhang et al. (2005) compared cloud properties simulated by general circulation models (GCMs) with those retrieved from satellite data for the Clouds and Earth's Radiant Energy System (CERES; Wielicki et al. 1996) Project and the International Satellite Cloud Climatology Project (ISCCP). Although they found that most GCMs underestimated midlatitude marine boundary layer (MBL) cloud fractions (CFs) and overestimated their optical depths, the GCMs computed relatively accurate top-of-the-atmosphere (TOA) radiation budgets because the errors in CF and optical depth offset each other. As concluded in Randall et al. (2007), "Cloud feedbacks have been confirmed as a primary source of inter-model differences, with low clouds making the largest contribution" and "systematic biases have been found in most models' simulations of the Southern Ocean." Hwang and Frierson (2013) used multiple historical GCM simulations to perform a global energetic analysis and found that negative cloud biases over the southern oceans are responsible for excessive precipitation in the same hemisphere, leading to the occurrence of a double ITCZ.

The Intergovernmental Panel on Climate Change (IPCC) recently released its Fifth Assessment Report (AR5), which was accepted but not approved in detail on 26 September 2013. This assessment included multiple GCMs, developed by approximately 20 climate modeling groups from around the world, with outputs gathered through phase 5 of the Coupled Model Intercomparison Project (CMIP5; Taylor et al. 2012). These GCMs simulate past and present climates and, when combined, serve as our best predictors of climate change and the future climate. Although many improvements have been made in CMIP5 (e.g., Klein et al. 2013; Jiang et al. 2012), clouds are still a significant source of error in climate models (e.g., Jiang et al. 2012; Dolinar et al. 2014) and global numerical weather prediction (NWP) models such as the National Centers for Environmental Predictions (NCEP) Global Forecast System (GFS; Yoo and Li 2012; Yoo et al. 2013). Cloud structural and optical properties are strongly dependent upon interactions between aerosol/cloud microphysics and cloud-scale dynamics that are unresolved in large-scale models. Furthermore, these intricate interactions involve the formation of precipitation and its effect upon cloud dynamics, turbulence, and entrainment. However, we still lack understanding of many key physical links between cloud properties and environmental conditions and need observations to accurately quantify the multivariate sensitivity of precipitation to cloud microphysical and macrophysical properties. Such studies are essential for the evaluation of both climate and process-based numerical models.

To further our understanding of the connections between cloud properties and their environment, this paper focuses on comparisons of observations with similar quantities from the National Aeronautics and Space Administration (NASA) Goddard Institute for Space Studies (GISS) Model E2 atmospheric GCM (GISS-E2). Although globally averaged CF simulated by the CMIP5 version of the GCM is closer to that from satellite observations (Schmidt et al. 2014) relative to its CMIP3 predecessor (Schmidt et al. 2006; Kennedy et al. 2010; Naud et al. 2010), the GISS-E2 GCM, like most other CMIP5 GCMs, underestimates MBL clouds over the subtropical marine stratocumulus regions and the southern midlatitude (SML) oceans (Stanfield 2012; Dolinar et al. 2014). Recent GISS-E2 runs, denoted as post-CMIP5, have newly updated turbulence (Yao and Cheng 2012) and moist convection (Del Genio et al. 2012) parameterizations that have yielded substantial improvements over the SMLs and moderate improvement in coastal areas where MBL clouds frequently occur. For this study, the SMLs have been defined as the region bounded between 30° and 60°S.

This study documents the comparisons of CFs and properties simulated by GISS-E2 CMIP5 and post-CMIP5 versions and NASA satellite observations. In detail, CMIP5 and post-CMIP5 simulated CFs and cloud water path (CWP) are compared with Clouds and the Earth's Radiant Energy System–Moderate Resolution Imaging Spectroradiometer (MODIS) edition 2 cloud results (Minnis et al. 2011a) and *Cloud–Aerosol Lidar and Infrared Pathfinder Satellite Observations* (*CALIPSO*) profiles (Kato et al. 2010). Model-simulated liquid and ice water paths (LWP and IWP) are compared with *CloudSat* results (Austin et al. 2009). Simulated precipitable water vapor (PWV) is compared to Advanced Microwave Scanning Radiometer for Earth Observing System (AMSR-E) retrievals (Wentz 1997), while both PWV and relative humidity (RH) profiles are compared with Atmospheric Infrared Sounder (AIRS) retrievals (Olsen et al. 2007a,c).

Section 2 describes in detail the CMIP5 and post-CMIP5 versions of the model, as well as the similarities and differences between the two versions. The NASA satellite data products used in this study, such as CERES-MODIS, *CloudSat–CALIPSO*, AIRS, and AMSR-E, are also described in section 2. Section 3 compares the model outputs with satellite observations with a detailed discussion about the possible reasons for their differences. The results are summarized in section 4.

2. Datasets and methodology

a. GISS-E2 CMIP5 and post-CMIP5 model runs

Monthly CMIP5 (C5) simulated GISS-E2 Atmospheric Model Intercomparison Project (AMIP) runs with prescribed sea surface temperatures (SSTs) were retrieved using the Earth System Grid Federation (ESGF) Program for Climate Model Diagnosis and Intercomparison (PCMDI) database at a horizontal resolution of 2° × 2.5° (latitude × longitude) with 40 vertical layers. While multiple simulations of each model are provided by the ESGF PCMDI database, this study uses the ensemble member designated r5i1p3, outlined in Taylor et al. (2012). The third version of model physics (p3) includes aerosol direct, semidirect, and first indirect effects, although differences in mean fields between this model version and the version with noninteractive aerosols (p1) are small (Schmidt et al. 2014). The minimum relative humidity at which clouds are formed is tuned in order to reach global mean radiative balance within the GISS GCM.

The Post-CMIP5 (P5) intermediate diagnostic data are provided by NASA GISS. This revised model is fundamentally identical to its C5 predecessor; however, two major parameterization changes have been made. The cumulus parameterization has been modified with increased entrainment and rain evaporation and changes in the convective downdraft as detailed in Del Genio et al. (2012). Stronger entrainment allows the new cumulus parameterization to produce Madden–Julian oscillation (MJO)-like variability (Kim et al. 2012). Increased entrainment and rain evaporation decrease convective drying and thus can cause a small local increase in water vapor and cloudiness, especially in regions where convective depth is most sensitive to entrainment.

The boundary layer turbulence parameterization has been modified as well in the P5 simulation (Yao and Cheng 2012). According to Yao and Cheng (2012), this new scheme differs in its computation of nonlocal transports, turbulent length scale, and PBL height, and shows improvements in cloud and radiation simulations, particularly over the subtropical eastern oceans and the southern oceans, despite the fact that the stratiform cloud parameterization itself is unchanged from the C5 version. These changes bring the model more in line with observations regionally. In particular, the combination of the deeper extratropical boundary layer and shallower tropical boundary layer in the P5 turbulence parameterization is expected to increase and decrease low cloud fraction in these two regions, respectively.

Parameterization changes in the P5 version of the model are expected to have internal feedbacks across all variables. For example, convection and turbulence parameterization changes discussed previously are expected to directly impact the amount of PWV within the atmosphere. Changes to PWV should impact RH, which is used within the model as a control for CF. These changes, as well as the atmospheric temperature, then directly affect amounts of simulated CWP, LWP, and IWP.

P5-simulated CFs are stratified into high- ($P < 440$ hPa), middle- ($440 < P < 680$ hPa), and low-level ($P > 680$ hPa) cloud fractions based on the ISCCP classifications presented in Rossow and Schiffer (1999). Combinations of CFs within similar layer classifications were performed in-house by NASA GISS for both the P5 and C5 simulations, ensuring a proper vertical CF comparison. Global averages are calculated using a cosine-of-latitude weighting scheme.

b. Satellite data

Errors in satellite retrieved results are not explicitly accounted for in the figures shown in this comparison. Although satellite retrievals do contain uncertainties and biases, they remain good tools for diagnosing model issues. For example, NASA CERES-MODIS-retrieved cloud properties have been extensively validated using a suite of ground-based observations and retrievals (Dong et al. 2008; Minnis et al. 2011b; Xi et al. 2010, 2014, manuscript submitted to *J. Geophys. Res.*). On the other hand, cloud fields retrieved from different satellite instruments or using different retrieval techniques give markedly different results (Stubenrauch et al. 2013). The reader should note that, given this caveat about satellite retrievals and uncertainty, the term ''bias'' is used in this paper in its simplest form, and represents the difference between the model and the observation. We make note of known satellite retrieval errors when interpreting these differences.

1) CERES-MODIS

This study uses the daytime CERES-MODIS (CM) synoptic radiative fluxes and clouds (SYN1) edition 3 dataset for global and regional cloud fraction and the SYN1 edition 2.6 dataset for daytime only cloud water path comparisons, both of which include the CERES edition 2 cloud properties (Minnis et al. 2011a). The SYN1 edition 2.6 dataset is used in lieu of edition 3 for CWP comparisons because of the relatively large uncertainties for nighttime CWP retrievals with CWP > 50 g m^{-2}. Note that CERES uses different algorithms to retrieve MODIS cloud properties than those used by the MODIS Atmosphere Science Team (MOD06) (Platnick et al. 2003) as discussed by Minnis et al. (2011b). The SYN1 data used in this study are regridded to the 2.0° latitude × 2.5° longitude grid of the GISS-E2. Given that SYN1 results do not differentiate liquid and ice CFs, and

that retrievals of CWP are for combined *Terra* and *Aqua* cloudy scenes only, the gridded SYN1 CWP results are recalculated by multiplying the original data by the respective cloud fraction to achieve water path retrievals for all scenes. More than 5 yr of SYN1 data are used in this study (March 2000–December 2005). The SYN1 cloud layers are stratified into low, middle-low, middle-high, and high classifications. Maximum overlap was assumed between middle-low and middle-high layers to achieve an ISCCP-like classification of low-, middle-, and high-level clouds.

The CM *Aqua* and *Terra* CF retrievals have been extensively compared with other observational data by Minnis et al. (2008), who documented a 7% uncertainty in CM global CF retrievals. The global mean CM edition 2 CF is among the lowest values from 12 different satellite retrievals that ranged from 0.56 to 0.73 (Stubenrauch et al. 2013). The mean CM low and high CFs, however, are close to the respective averages for the 12 datasets. Thus, other than having lower midlevel cloud fractions than all other retrievals, except for *CALIPSO*, the CM CFs are fairly representative of passive satellite cloud amounts.

Dong et al. (2008) documented uncertainties in the CM retrieved cloud LWP and found mean LWP differences of $11.3 \pm 51.0\,\mathrm{g\,m^{-2}}$ compared to U.S. Department of Energy (DOE) Atmospheric Radiation Measurement Program (ARM) ground-based microwave radiometer retrieved LWPs at the Southern Great Plains Central Facility. Minnis et al. (2011b) found that the CM LWP over ocean was, on average, $0.2 \pm 53.6\,\mathrm{g\,m^{-2}}$ less than LWP from matched overcast AMSR-E footprints. For single-layer cirrus clouds, Mace et al. (2005) found that the CM IWP was $3.3 \pm 16.2\,\mathrm{g\,m^{-2}}$ less than IWP derived from a ground-based radar. Although not quantified precisely, the CM IWP means for all ice clouds are similar in magnitude and distribution compared to IWP from *CloudSat* (Waliser et al. 2009). Minnis et al. (2007) found that for ice-over-water cloud systems, CWP from the single-phase retrieval (CWP = IWP) was 10%–15% greater than when IWP and LWP were retrieved explicitly using microwave and visible-infrared imagers together. Thus, in these situations, the CM IWP (CWP) is probably overestimated by 10%–15%. Further discussion of the CM cloud properties uncertainties is found in Minnis et al. (2011b).

2) *CloudSat–CALIPSO*

The *CALIPSO* and *CloudSat* satellites were launched in April 2006 as part of the A-Train constellation (Winker et al. 2007). *CALIPSO* carries the Cloud–Aerosol Lidar with Orthogonal Polarization (CALIOP) instrument, a nadir-viewing two-wavelength (1064 and 532 nm) polarization lidar. The *CloudSat* millimeter wavelength cloud profiling radar (CPR) has the unique ability to observe the majority of cloud condensate and precipitation within its nadir field of view. The *CloudSat*-retrieved properties have a vertical resolution of 500 m (Stephens et al. 2002). When combined with *CALIPSO*, they yield a nearly complete vertical cloud profile, the exception being hydrometeors in the lower troposphere that may be masked because of attenuation or surface clutter (Marchand et al. 2008).

Four years of *CloudSat–CALIPSO* (CC) data, from July 2006 to June 2010, are used in this study. The CALIOP and CPR retrievals from the *CALIPSO–CloudSat*–CERES–MODIS (CCCM; Kato et al. 2010) RelB1 data product are used for total column CF comparisons. The *CloudSat* water content retrievals are provided by the Jet Propulsion Laboratory (JPL), described in Austin et al. (2009), and are used for liquid, ice, and total cloud water path comparisons. The *CALIPSO* and *CloudSat* retrievals are averaged on the GISS-E2 grid. Maximum overlap was used to stratify CFs into high-, middle-, and low-level cloud fraction using vertical CF profile retrievals. Surface-based radar analyses suggest departures from maximum overlap even over distances of a few kilometers (Hogan and Illingworth, 2000), so these may be lower bounds on the actual CF values for each cloud type.

3) AIRS

This study uses more than 10 yr (January 2003–December 2012) of level 3 AIRS products including version 5 PWV data (Olsen et al. 2007c) and version 6 RH data (Olsen et al. 2013). AIRS is one of the six instruments on board the *Aqua* satellite with a spatial resolution of 50 km and 12 layers. Both PWV and RH are regridded to the GISS-E2 grid. PWV retrievals are more reliable from 1000 to 300 hPa over ocean, and from 850 to 300 hPa over land, with an estimated uncertainty of 25% in the tropics, 30% within the midlatitudes, 50% at high latitudes, and 30% globally averaged (Jiang et al. 2012). Because AIRS cannot retrieve water vapor amounts in largely overcast scenes, which are usually more humid than clear scenes, it is dry-biased by 5%–10% over much of the globe; the opposite is true in subtropical stratocumulus regions in which near-overcast scenes are overlain by very dry air (Fetzer et al. 2006). The uncertainties in the AIRS-retrieved RH profiles in conjunction with the temperature profiles can be within 10% in 2-km layers and about 50% in the upper troposphere, with an estimated uncertainty of 15%–25% for the entire atmosphere (Fetzer et al. 2006). The AIRS SST retrievals have an estimated uncertainty of 1.0 K between ±50° latitudes (Olsen et al. 2007a). In this study,

the GISS-E2 RH profiles are interpolated down to 12 layers to match the AIRS vertical resolution. An attempt was made to derive SST from available surface skin temperatures; however, this method has been substituted for using surface air temperature over water as an estimate of SST on account of the noise found in the surface skin temperature parameter.

4) AMSR-E

Nine years (July 2002–July 2011) of AMSR-E level 3 version 5 PWV data are used in this study (Wentz 1997). The data were obtained from Remote Sensing Systems (http://www.remss.com) in their native gridded resolution of 0.25° × 0.25°. The product is estimated to have a random error up to approximately 1.2 kg m^{-2}. For the comparisons, AMSR-E PWV data were transposed to the GISS-E2 grid. The AIRS and AMSR-E PWV data over the oceans have been extensively compared by the AIRS science team, described in Fetzer et al. (2006), who found a difference of no more than 5% when both instruments view the same scene. The AMSR-E PWV retrievals over oceans are higher than their AIRS counterparts simply because AMSR-E is capable of measuring PWV from the surface to TOA, while reliable AIRS retrievals are restricted from 1000 to 300 hPa, and also because of the dry bias resulting from the omission of nearly overcast scenes described above.

The *CloudSat–CALIPSO* and CERES-MODIS results are provided in tandem for comparison with GISS-E2 atmospheric model data to assess the model results against both active and passive observations. The CPR and CALIOP instruments sample clouds and aerosols directly, detecting thinner clouds at a higher resolution but over a smaller coverage area, whereas CERES-MODIS indirectly measures clouds and aerosols over a broader area. Given that all observations have a level of uncertainty, the modeled data are compared to these two datasets in tandem to also help alleviate doubt from uncertainty and essentially provide an upper and lower bounds of what is considered truth. Much like *CloudSat–CALPISO* and CERES-MODIS, AIRS and AMSR-E are provided in tandem because of their complimenting strengths. The AMSR-E retrievals are valid for the full column of the atmosphere, but are limited to ocean-only retrievals, while the AIRS retrievals are provided over both land and ocean, but are restricted from 1000 to 300 hPa. As such, AMSR-E will be more reliable for comparisons over the ocean, while AIRS should be considered over land.

3. Results and discussion

a. Cloud fraction

Figures 1a–d show observed and modeled gridded annual CFs for CM, CC, P5, and C5 results, respectively, while Figs. 1e–h show the differences between simulated and observed CFs (P5 − CM, C5 − CM, P5 − CC, and C5 − CC, respectively). Comparing two observational datasets, the annual global average of CC derived CF is approximately 12% higher than CM, with much higher values over the Arctic regions. This discrepancy is a result of different sensitivities to clouds between passive and active remote sensing; CC is more sensitive to optically thin and small clouds while CM has a tendency to miss small cumulus and clouds with optical thicknesses less than 0.3 (Chiriaco et al. 2007; Minnis et al. 2008). The CF differences between CM and CC can be reduced to within about 2% if CC-derived CFs (~63%) are limited to clouds with optical depth greater than 0.3 (not shown in this study).

Although the global average P5 and C5 simulated mean CFs agree within 1%, significant differences are evident over some regions, such as the Arctic and SMLs (Figs. 1c,d). The P5 and C5 simulated global distributions and mean CFs agree much better with CM than with CC, suggesting that the GISS GCMs cannot simulate some of the optically thin clouds ($\tau < 0.3$) observed by CC. The C5 simulated CFs are greater than the CM CFs over the tropical and polar regions, but lower over the midlatitudes (Figs. 1a,d). The newly simulated CFs from P5 agree much better with the CM CFs, especially over the midlatitudes, but without significant improvement over the tropical Pacific Ocean (Figs. 1a,c). Arctic comparisons are not strongly considered at the time of this study given the known low biases associated with Arctic CM observations (Chiriaco et al. 2007; Minnis et al. 2008), as well as latitudinal limitations of CC observations (Winker et al. 2007). MBL clouds are dominant over the SML regions as illustrated in Fig. 2d. While large improvements were observed in MBL CFs over the SMLs in Fig. 1, the P5-simulated CFs over regions with a high occurrence of subtropical MBL clouds, such as off the coasts of Peru and California, have only increased moderately.

Figure 2 shows zonally averaged total and low/middle/high CFs derived from observations and simulations. As expected, CC-derived total CFs are higher than the CM and model-simulated CFs over both the tropics and midlatitudes (60°S–60°N) and agree well with model simulations over the polar regions (60°–90° latitude in both hemispheres), while the CM-derived total CFs are approximately 20% lower than the other three datasets over the polar regions (Fig. 2a). Over the SMLs, the P5 total column CFs agree with CM and CC observations better than the previous C5 results because of the implementation of the new PBL scheme in P5. The changes to the PBL scheme deepen the boundary layer in the extratropics and result in an increase of low-level CFs (Fig. 2d). Over the tropics, the P5 simulated total

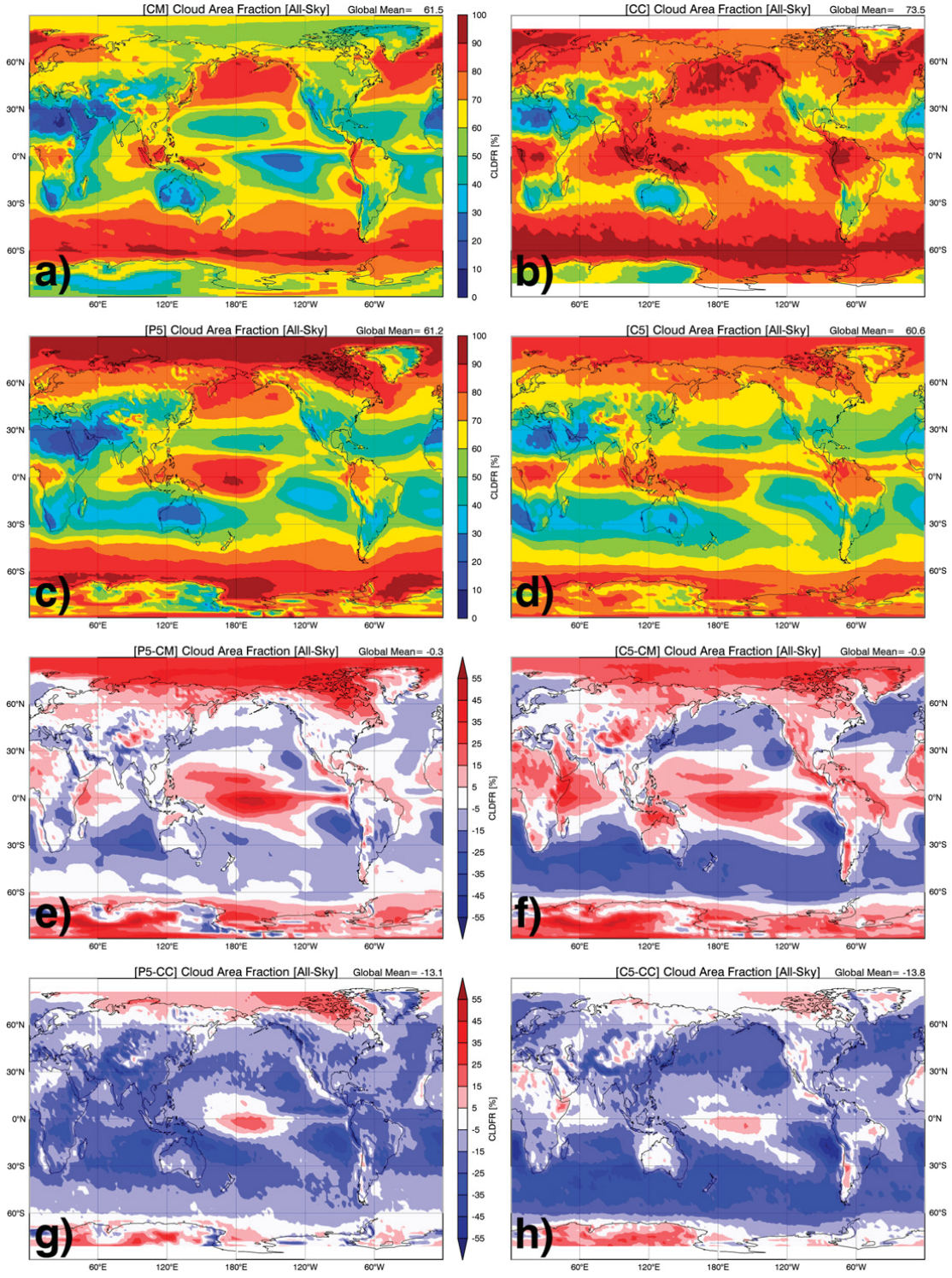

FIG. 1. Gridded annual mean CFs derived from (a) NASA CM results, (b) NASA CC observations, and simulated by NASA GISS (c) P5 and (d) C5 GCM simulations, as well as their differences, (e) P5 − CM, (f) C5 − CM, (g) P5 − CC and (h) C5 − CC, for the period of March 2000 through December 2005.

column CFs are slightly lower than the previous C5 results, primarily as a result of the shallower tropical boundary layer in P5 relative to C5 in tropical regions outside the marine stratocumulus decks. For both high and midlevel CF comparisons, P5, C5, CC, and CM all agree well each other, with the exception of the CM-derived CFs, which are lower than the others, particularly over the Arctic regions (Figs. 2b,c).

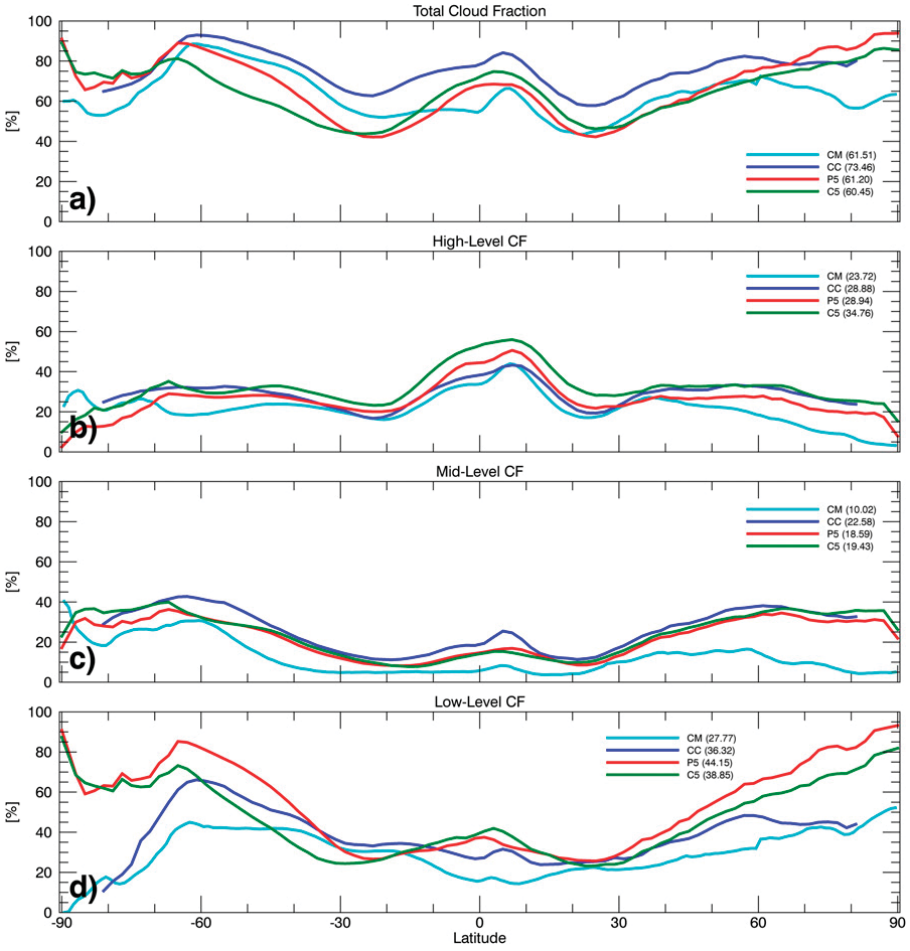

FIG. 2. Zonally averaged (a) total CF and (b) high- ($P < 440$ hPa), (c) mid- ($440 < P < 680$ hPa), and (d) low-level ($P > 680$ hPa) CFs from NASA CM and CC observations and NASA GISS P5 and C5 simulations. Values in parentheses indicate corresponding global means.

b. *Water path*

The layouts of Figs. 3 and 4 are essentially the same as in Figs. 1 and 2; however, Fig. 3 describes observed and simulated CWPs whereas Fig. 4 breaks down CWP by phase and relates these properties to total column CF. As illustrated in Figs. 3a, 3b, and 4b, the *CloudSat* (CS) and daytime CM retrieved global CWP distributions and their annual means are similar to each other with some exceptions. For example, the CS-derived CWPs over the tropics are almost doubled those retrieved from CM. Over marine stratus regions, however, the CM values are about 50 g m^{-2} more than the CS values resulting from the limitation of CS for detecting clouds below 1 km. These discrepancies result in approximately 16 g m^{-2} more globally averaged CWP retrieved from CS than from CM. Although the overall global CWP distributions from both P5 and C5 are fairly similar to CM and CS, their global mean CWPs are much higher than both CM and CS, primarily as a result of the oversimulation of CWPs over the tropics. However, the P5-simulated CWPs over the tropics are much lower than the previous C5 results, bringing results from the new version of the model closer to observations. This improvement directly reflects the shallower tropical boundary layer in P5. Over the tropics, the decrease in CWP from the C5 to the P5 version is consistent with the decrease observed in total column CF, whereas comparing CWP and total column CF over the SMLs shows the opposite relationship. For example, the MBL CFs simulated by the P5 version of the GCM are about 20% higher than the C5 results, while the P5-simulated CWPs are 25 g m^{-2} less than the C5 results. This small change may be an artifact; the CWP diagnostic in the GCM is for stratiform clouds only. P5 has more frequent shallow convection than C5 in the SMLs (Fig. 7 of Yao and Cheng 2012), causing an apparent decrease since its cloud water is not accounted for in CWP.

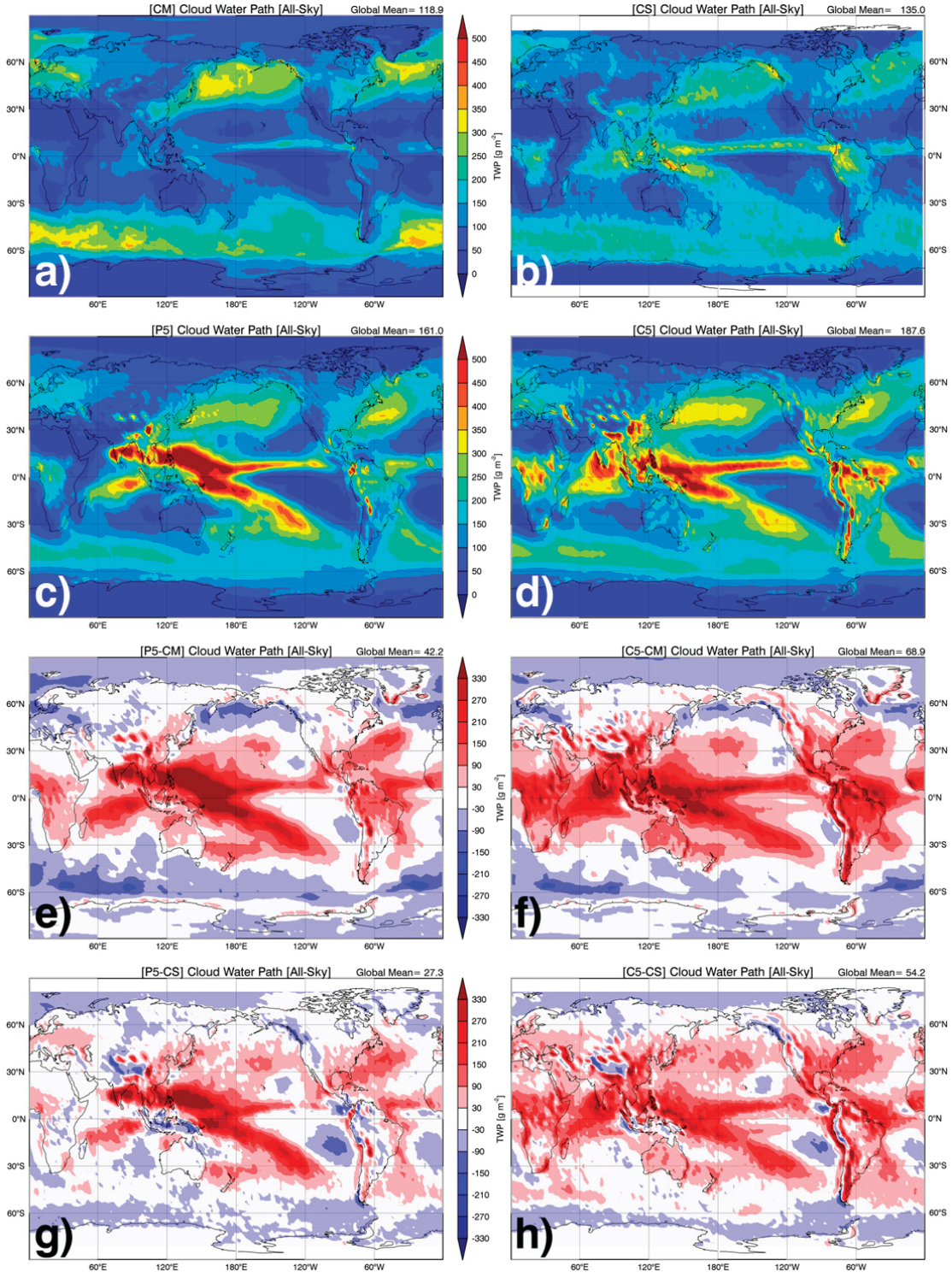

FIG. 3. As in Fig. 1, but for CWP.

To understand the partitioning between ice and water, cloud LWP and IWP comparisons are shown in Figs. 4c and 4d, respectively. Note that the CM results are not shown in Figs. 4c and 4d because portions of the SYN1 LWP are hidden under ice and deep convection clouds, making the separation of water path into LWP and IWP unreliable. The P5-simulated LWPs are consistently much lower than those simulated from C5 by roughly 25–50 g m^{-2}, and are close to the CS retrievals, particularly over the SML region (Fig. 4c). Figure 4d shows

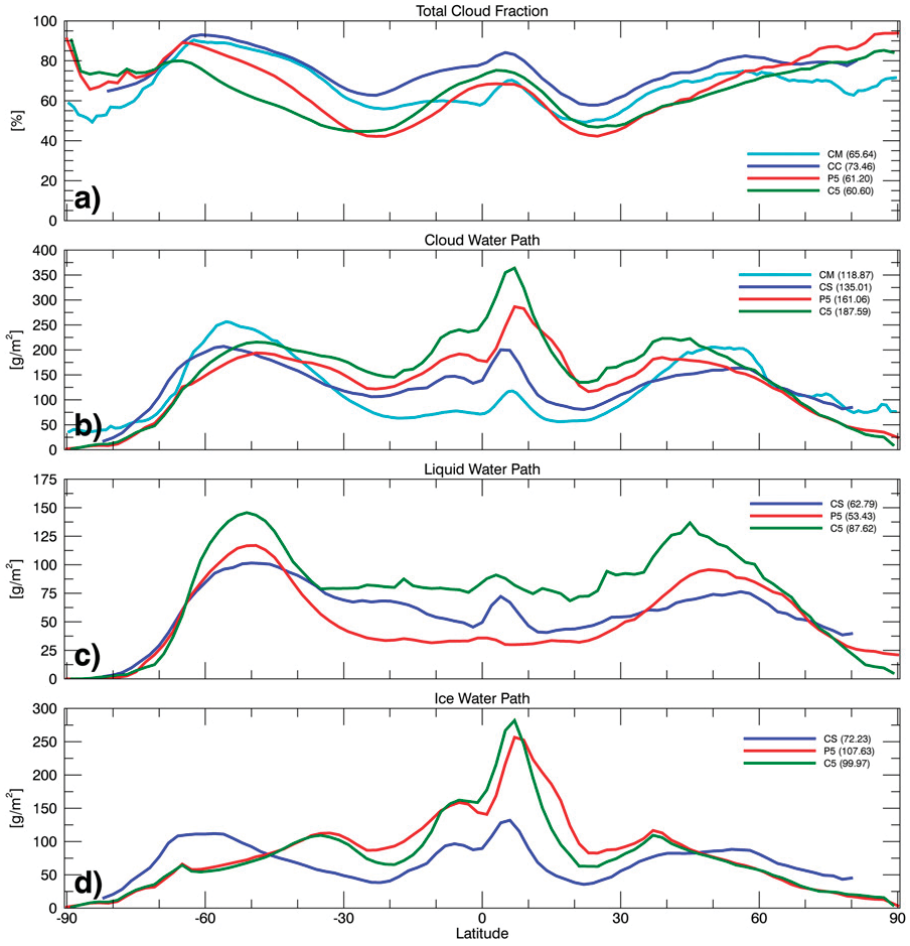

FIG. 4. Zonally averaged (a) total CF (daytime only for CM), (b) CWP (daytime only for CM), (c) LWP, and (d) IWP. Values in parentheses indicate corresponding global means.

that both the P5 and C5 simulated IWPs are roughly 100–200 g m^{-2} higher than the CS results over the tropical regions, with a peak at around 5°N that is several degrees offset from the CS maximum.

c. *Precipitable water vapor*

Figure 5 shows observed and simulated PWV means from AIRS, AMSR-E, P5, and C5, respectively, and the differences between simulated and observed PWV values. The AMSR-E PWV retrievals are slightly higher than the AIRS retrievals over the Indonesia–Papua New Guinea area. Given the limitations of each instrument, this is expected considering AIRS retrieves PWV between 1000 and 300 hPa over ocean, and from 850 to 300 hPa over land, but only in scenes with significant clear sky, while AMSR-E is able to perform PWV retrievals from the surface to TOA in virtually all cloud conditions. Of the two, the AMSR-E PWV retrievals are more reliable than AIRS data over the ocean.

The global P5 and C5 simulated PWV patterns match well with the observed patterns, with the maximum occurring in the tropics along the ITCZ. As demonstrated in Figs. 5 and 6, P5-simulated PWV values are higher than both C5 and AIRS results by as much as 11 g m^{-2} over the tropical regions, because of stronger convective rain evaporation occurring in the P5 version of the model. Although the overall C5 global PWV pattern and mean matches well with the AIRS observations (Figs. 5a,d), the C5 PWV values are less than the AIRS values by as much as 9 g m^{-2} over land (Fig. 5f). These discrepancies have been reduced significantly in the P5 simulations (Fig. 5e). Given that AIRS contains a dry bias resulting from AIRS being unable to perform retrievals during overcast conditions, along with instrument limitations discussed above, the P5 simulations make more physical sense than the C5 results over land. Over the ocean, the C5-simulated PWV values have negative biases of 1–5 g m^{-2} globally except for within a small region over the tropical Pacific Ocean, whereas P5 results agree better with AMSR-E retrievals globally, excluding over the tropical Pacific Ocean. Over the SMLs, the P5 PWV results more closely resemble

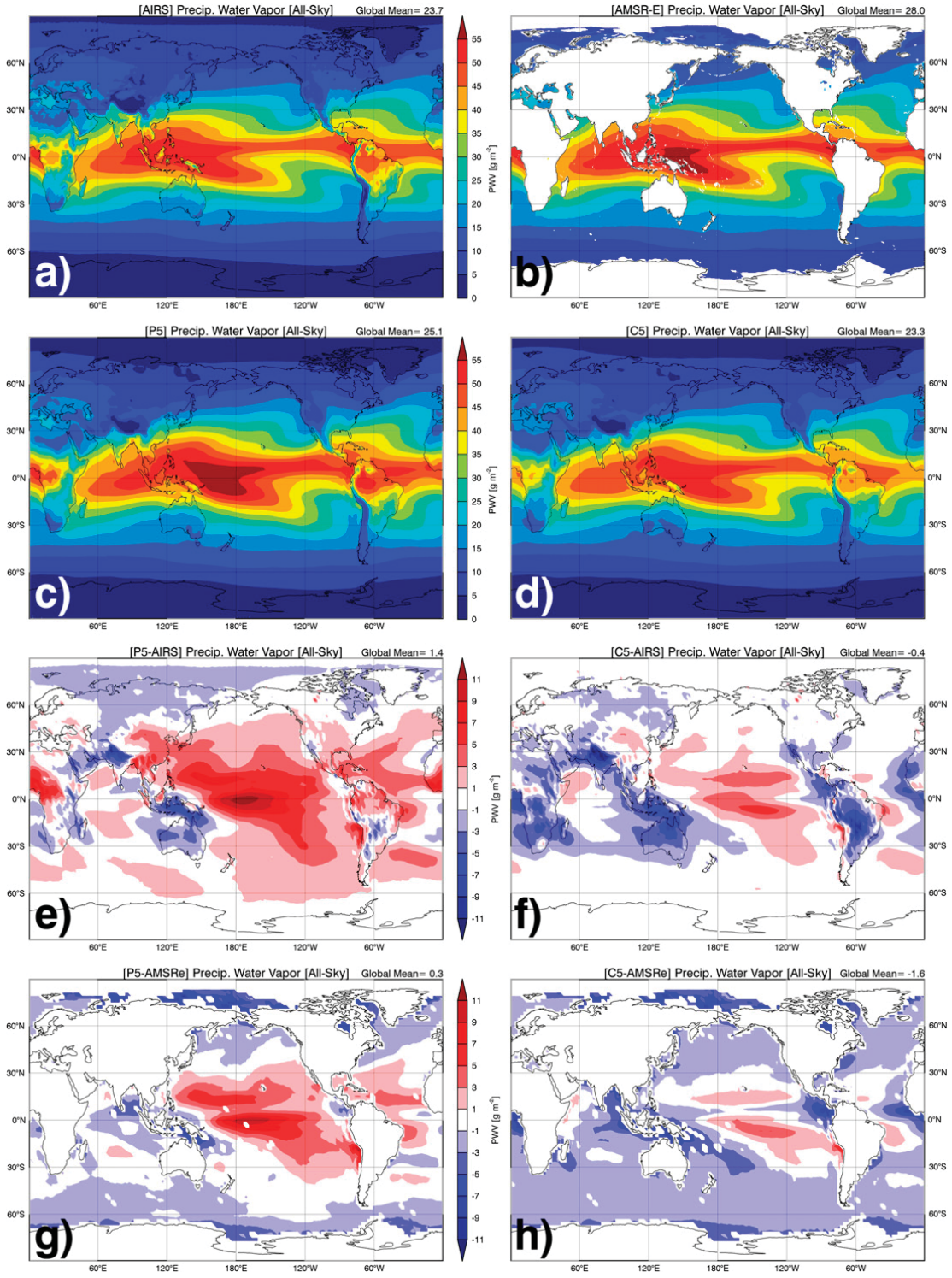

FIG. 5. As in Fig. 1, but for PWV derived from AIRS and AMSE-R observations, as well as simulated by NASA GISS P5 and C5.

AMSR-E observations than C5 results, which provides strong support for P5 simulating more MBL clouds than C5 (Figs. 1c and 2d) given the same SST and cloud microphysical schemes in both P5 and C5.

Zonally averaged PWV and SSTs are presented in Fig. 6. It worth noting that surface air temperature over water was used as an estimate for AIRS SST because of the noise found in its surface skin temperature

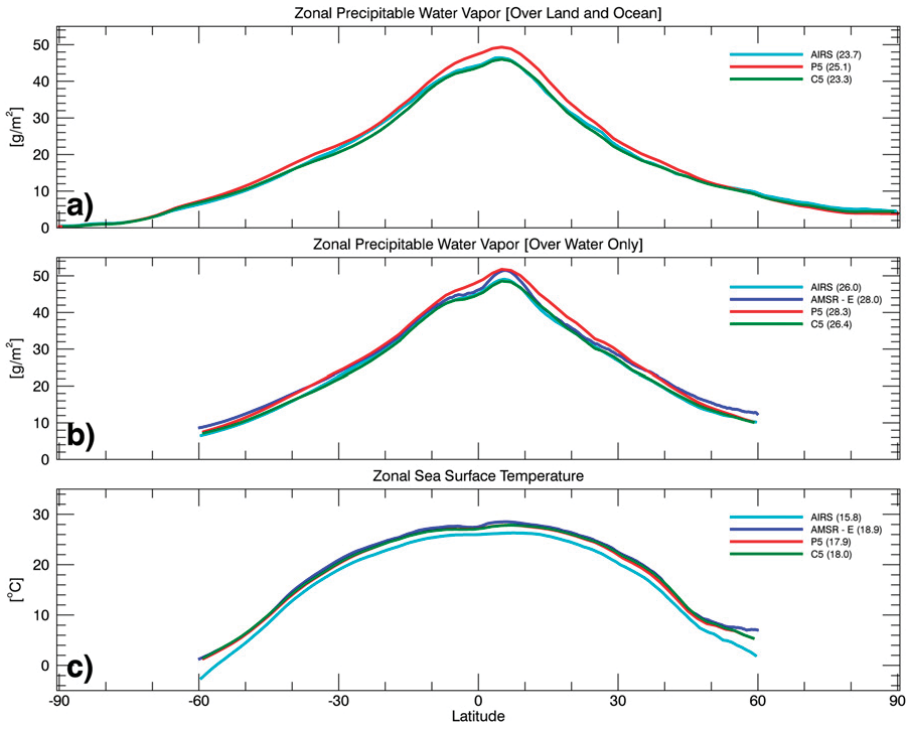

FIG. 6. Latitudinally averaged PWV (a) over both land and ocean and (b) over ocean only, and (c) SST. Note that AMSR-E has results only over ocean. Values in parentheses indicate corresponding global mean.

retrievals. As illustrated in Fig. 6a, P5-simulated PWV values are higher than AIRS retrievals, while the C5 results closely match AIRS retrievals. Differences between P5 and AIRS increase in intensity approaching the equator from the midlatitudes, on the order of $3\,g\,m^{-2}$. This makes physical sense given the dry bias associated with AIRS retrievals. By limiting zonally averaged PWV values to those only over the ocean (Fig. 6b), the comparison shows a close correlation between P5 simulations and AMSR-E retrievals, maintained within $2\,g\,m^{-2}$. Figure 6c indicates that the prescribed SSTs used in C5 and P5 simulations are consistent with AMSR-E observations. The model-prescribed SSTs are fairly consistent with those from AIRS, given that surface air temperature over water was used as an estimate of SST. The P5 PWV values over the ocean are close to both the AMSR-E and AIRS results, but higher than the C5 simulations.

d. Relative humidity

Given the central role of RH in many climate models as a regulator of clear-sky outgoing longwave radiation and an indicator of when clouds will form, it is important to assess this property against observations. Figures 7a–c illustrate the AIRS, P5, and C5 RHs, while Figs. 7d and 7e show the differences between the AIRS and the P5 and C5 RH profiles.

Comparisons of the GISS GCM and AIRS RH averages initially are possible only for the lowest portion of the atmosphere, because of differing definitions of RH in the model diagnostic and the AIRS product. The AIRS algorithm calculates RH based on liquid saturation when temperature $T > 0$°C and switches to ice saturation when $T < 0$°C (Olsen et al. 2007b), while the model calculates RH relative to a saturation reference value that varies with temperature when $T < 0$°C but saves its RH diagnostic based on a constant liquid saturation reference throughout the atmosphere. To make a correct RH comparison, RHs from the GISS GCM have been rescaled by applying the same method as AIRS, using Eqs. (7), (10), and (11) in Murphy and Koop (2005).

As demonstrated in Figs. 7b and 7c, both global and vertical RH distributions, the P5 RHs are moister than the C5 values. Regionally, both the P5 and C5 RH patterns are wetter than the AIRS retrievals over the tropics, slightly more so in P5 than in C5. Most of this difference can be ascribed to the AIRS dry bias. Over the SMLs, the P5 and C5 low-level RHs are about 10% greater and less than the AIRS retrievals, respectively (Figs. 7d,e). This finding is consistent with the CF comparison and provides strong support for the increase in the number of low-level clouds being simulated by P5 over the SML region (Figs. 1 and 2). Over the polar

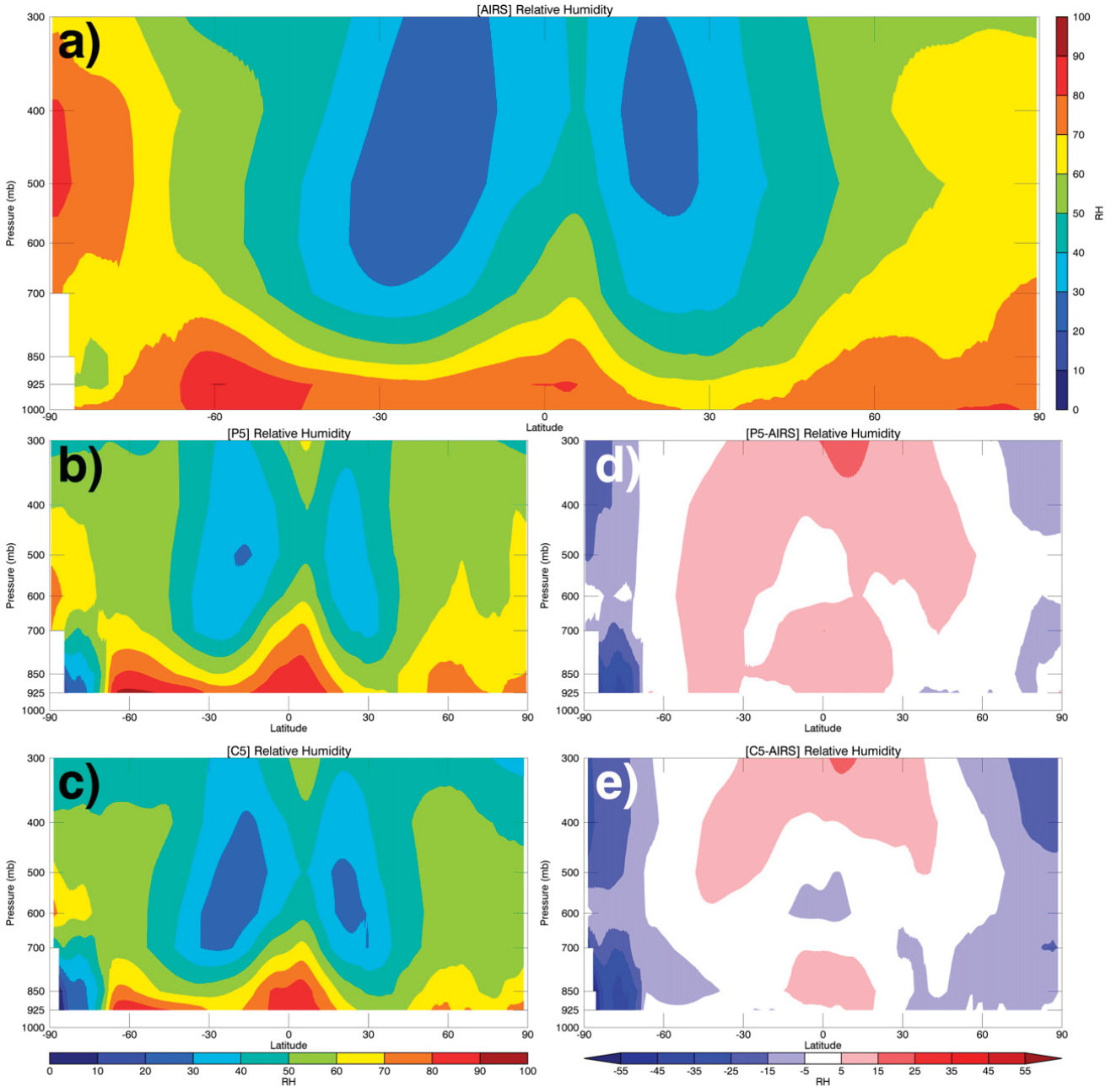

FIG. 7. Vertical distributions of RH derived from (a) AIRS observations, and by NASA GISS (b) P5 and (c) C5 simulations, as well as the differences between AIRS and (d) P5 and (e) C5.

regions, better agreement is found between the P5 and AIRS RH means, particularly within the Arctic. Mean RH and temperature profiles for P5, C5, and AIRS have been plotted in Fig. 8 over the tropical, midlatitude, and polar regions. Each RH profile is consistent with the results shown in Fig. 7 and serves as a quick glance summary of RH over each respective region. The temperature profiles in Fig. 8 compare well with the RH results, with higher temperatures corresponding to lower RH values. Overall, we find consistent temperatures in the upper levels of the atmosphere, particularly in the tropics. In the midlatitude and polar regions, deviation occurs in the temperature profiles below 700 and 600 hPa, respectively.

e. *Spatial and variability analysis using Taylor diagrams*

Taylor diagrams (Taylor 2001) have been generated using standard deviations and correlations to compare the P5/C5 GCM simulations with the observational datasets in this study. These results are illustrated in Figs. 9a–d, comparing the P5 and C5 simulations versus

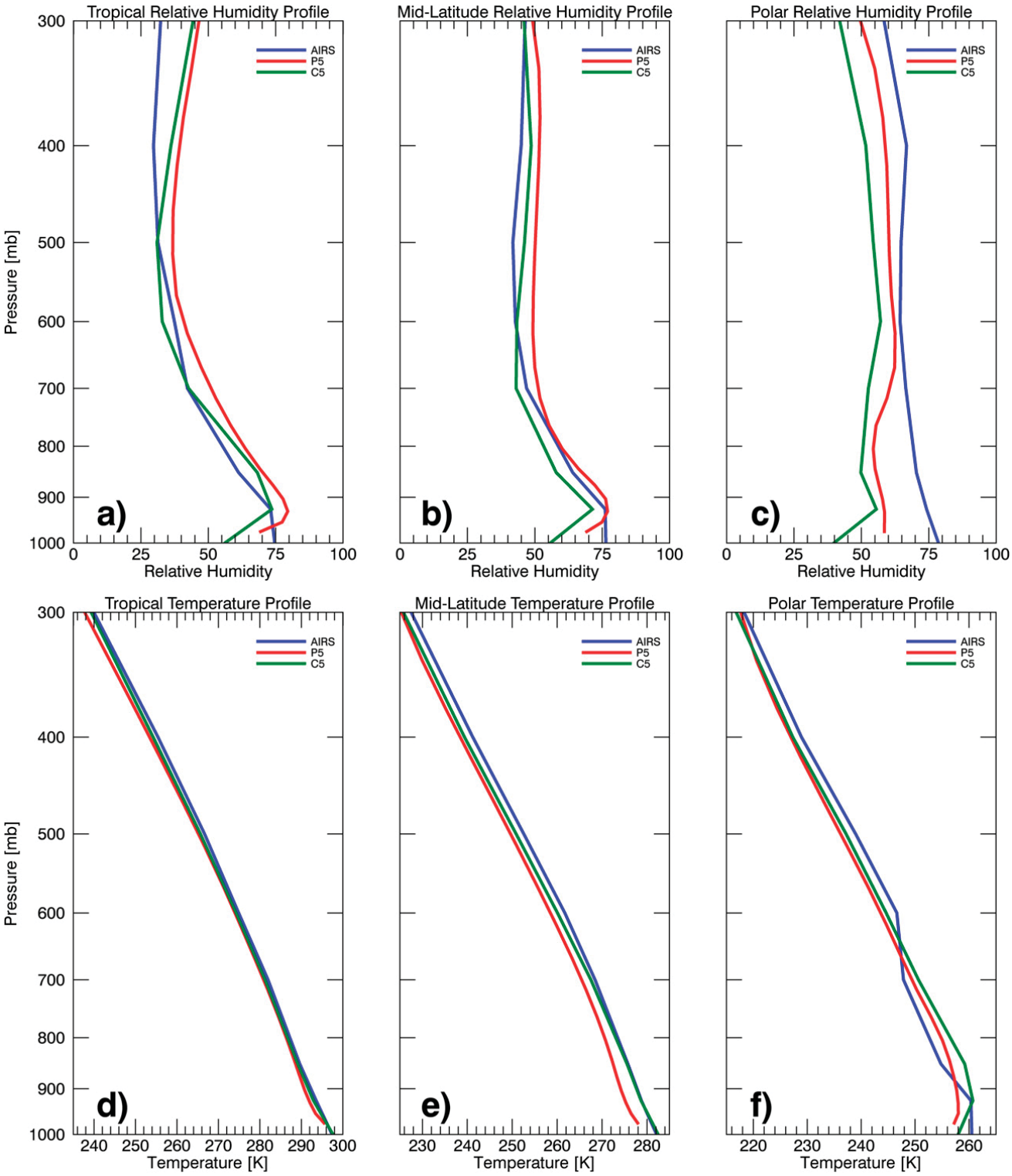

FIG. 8. Vertical distributions of (top) RH and (bottom) temperature from AIRS and NASA GISS P5 and C5 simulations over (a),(d) tropical (30°S–30°N), (b),(e) midlatitude (30°–60° lat both hemispheres), and (c),(f) polar regions (60°–90° lat both hemispheres).

the CM, CC, AIRS, and AMSR-E retrievals, respectively. Taylor diagrams are a convenient way to summarize differences in mean geographic patterns between models and observations. It should be noted, however, that with the occasional exception such as the SML ocean cloud bias (Trenberth and Fasullo 2010), most model–data intercomparisons have found no obvious relationship between fidelity of model geographic patterns

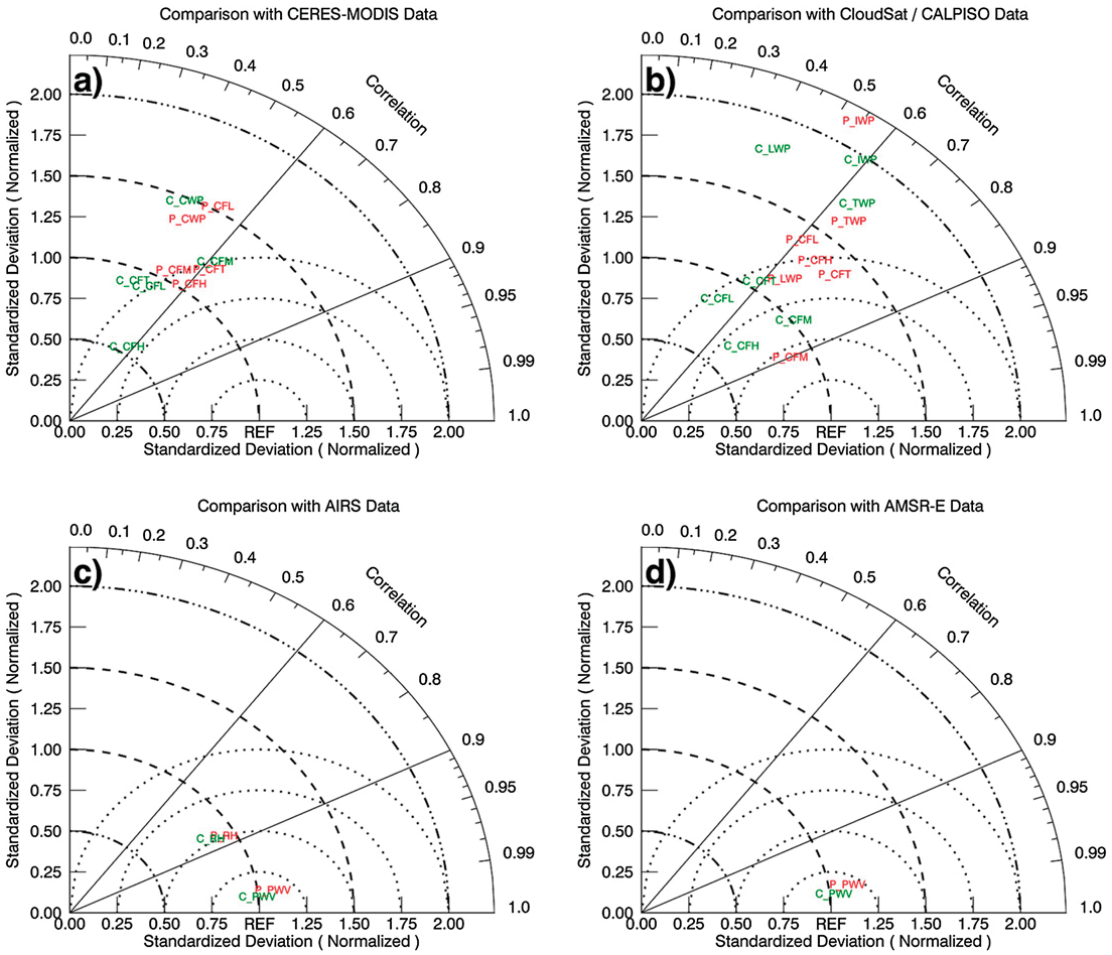

FIG. 9. Taylor diagrams comparing P5 and C5 variables with (a) CM, (b) CC and CS, (c) AIRS, and (d) AMSR-E observations.

and their predictions of climate change (Pincus et al. 2008; Collins et al. 2011; Klocke et al. 2011). For example, the global climate sensitivities of the C5 and P5 models to a doubling of CO_2 are identical at 2.9°C.

Note that the radii in Fig. 9 are given as normalized standard deviation, calculated for each variable as the standard deviation of the GCM simulation divided by the standard deviation of the observation. If the model simulations agree with observations as well as can be expected given observation retrieval errors, different time periods covered by the data and model, and internal variability of the climate system, then the simulated results would be located close to the reference point (REF) at one standard deviation and with a correlation about 1 on the diagram. Such is the case for the PWV comparisons between the model and AMSR-E retrieved PWVs in Fig. 9d, as well as with AIRS-retrieved PWV and RH comparisons in Fig. 9c. The P5 and C5 simulations are moderately correlated (~0.5–0.8) with the CC and CS results but with large standard deviations (1–2σ), whereas the P5 and C5 simulations are much less correlated (0.2–0.6) with the CM results and have low standard deviations (~1σ). Comparing to all observational datasets, the P5 correlations increase slightly relative to C5 simulations. Note that the correlations and standard deviations in Fig. 9 are relative values given that the observational datasets have some uncertainties, some of which are very large.

f. *Quantitative estimation of improvement in CFs and cloud properties over the SMLs*

To quantitatively estimate the improvements in modeled CFs, scatterplots between CM and CC observed and P5 and C5 simulated CFs globally and over the SMLs are shown in Fig. 10. Within these scatterplots, each point/dot represents the annual average of a single grid point within the region of interest, be it globally or restricted to the SMLs. Global comparisons of P5 and C5 simulations to CM (Fig. 10a) and CC (Fig. 10b) both show an improvement in the P5-simulated total column CF. Root-mean-square error (RMSE) values have decreased slightly, while linear regressions of the data

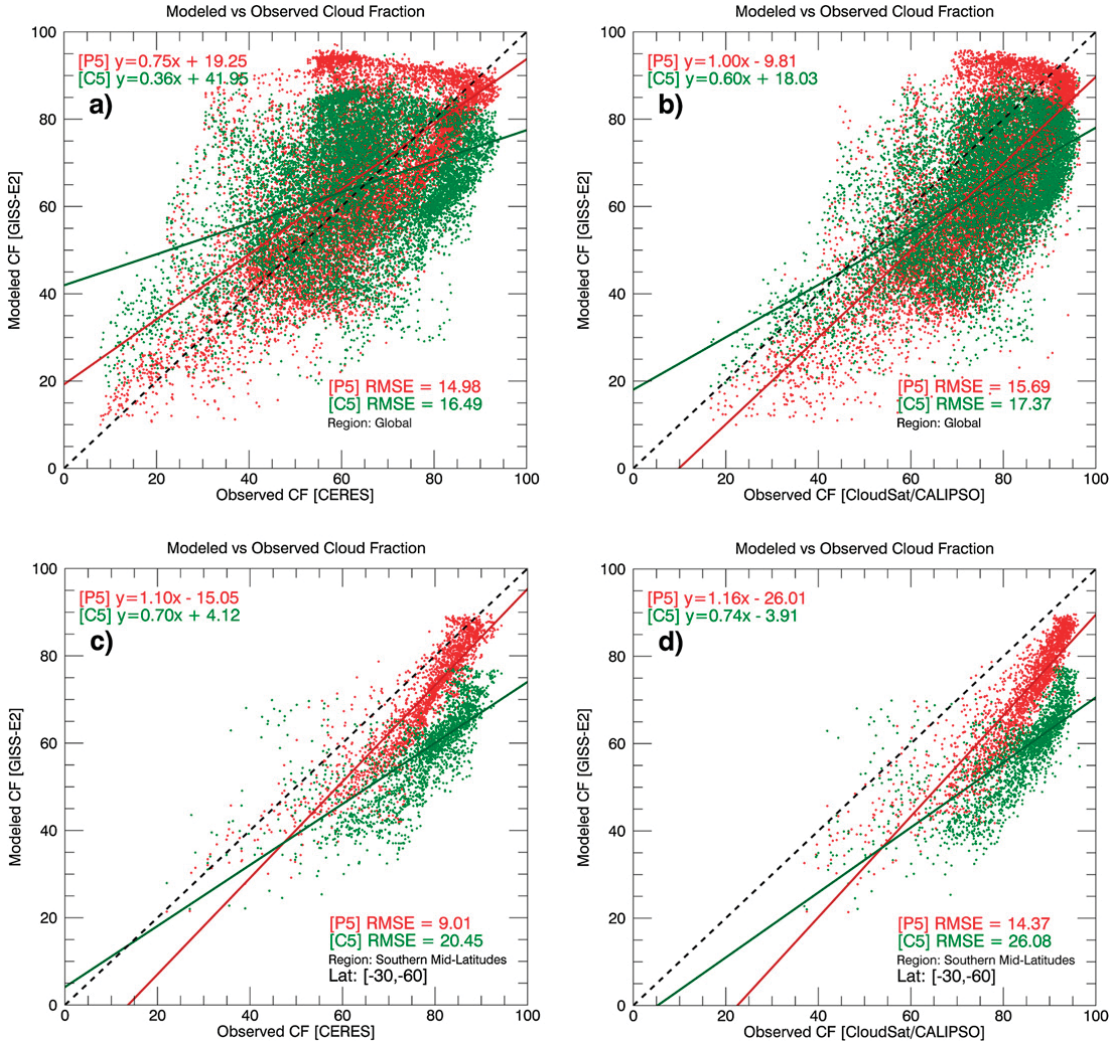

FIG. 10. Scatterplots and associated linear regressions and RMSE of simulated and observed total column cloud fraction both (a),(b) globally and (c),(d) restricted within the SMLs; comparing the models with (left) CERES and (right) *CloudSat–CALPISO* observations, respectively.

more closely resemble a one-to-one relationship with the observations. Within the SML focus region, parameterization changes in the P5 model, particularly changes to the boundary layer turbulence parameterization, have roughly halved RMSE values between the model runs when compared with both CM (Fig. 10c) and CC observed total column CFs (Fig. 10d).

To provide a more objective and quantitative comparison between the model simulations against observations, Tables 1 and 2 have been generated to show the global and SML bias, RMSE, and correlation between each model and observation for all variables presented in this study. As demonstrated in Tables 1 and 2, while some improvements were made in the P5 simulation on a global scale, large improvements have been found within the SML focus region. For example, the correlations in total column CF between the P5 simulation and observations increase from global correlations of 0.64 and 0.75 to 0.9 within the SMLs, and a stronger reduction in bias and RMSE is found over the SMLs. P5-simulated total column CFs also have higher correlations than C5-simulated total column CFs (0.75) and their bias and RMSE are nearly half of the C5 results. Comparing CC-observed CFs at all levels, the P5 simulations also make much more improvement over the SMLs given the strength of CC to penetrate the upper cloud layers and see more clouds at the lower levels. The P5 simulation also shows better agreement in CWP and LWP with the observations, as well showing a good agreement with AMSR-E retrieved PWV.

4. Summary and conclusions

NASA GISS-E2 CMIP5 (C5) and post-CMIP5 (P5) simulated cloud fractions and cloud properties were assessed utilizing observed satellite products from CERES-MODIS,

TABLE 1. Global comparison of bias, RMSE, correlation, and standard deviation, between simulated and observed variables. The last column serves as a quick lookup table, displaying if the bias, RMSE, and correlation in the P5 simulation improved (I), worsened (W), or remained constant (—), respectively, in relation to each dataset compared to its C5 predecessor.

Variable	Model	Observation	Bias	RMSE	Correlation	Quicklook
CF (total; %)	P5	CM	−0.3	14.98	0.64	I, I, I
	C5	CM	−0.9	16.49	0.39	
	P5	CC	−13.0	15.69	0.75	I, I, I
	C5	CC	−13.6	17.37	0.59	
CF (high; %)	P5	CM	5.1	11.74	0.63	W, W, I
	C5	CM	−2.9	10.02	0.58	
	P5	CC	−0.3	9.40	0.68	I, I, W
	C5	CC	−8.3	10.18	0.75	
CF (mid; %)	P5	CM	8.5	13.74	0.58	W, W, —
	C5	CM	3.0	10.04	0.58	
	P5	CC	−4.2	6.89	0.90	I, I, I
	C5	CC	−9.7	12.51	0.80	
CF (low; %)	P5	CM	16.2	30.20	0.57	W, W, I
	C5	CM	−7.0	16.33	0.44	
	P5	CC	7.4	22.36	0.61	I, W, I
	C5	CC	−15.8	21.51	0.49	
CWP ($g\,m^{-2}$)	P5	CM	42.3	99.23	0.46	I, I, I
	C5	CM	68.9	111.95	0.43	
	P5	CS	26.0	78.77	0.67	I, I, I
	C5	CS	52.6	90.46	0.65	
LWP ($g\,m^{-2}$)	P5	CS	−9.7	29.62	0.64	I, I, I
	C5	CS	24.6	57.5	0.38	
IWP ($g\,m^{-2}$)	P5	CS	35.3	84.68	0.54	W, W, W
	C5	CS	27.7	73.82	0.59	
PWV (all; $g\,m^{-2}$)	P5	AIRS	1.4	2.45	0.99	W, W, —
	C5	AIRS	−0.4	1.76	0.99	
PWV (ocean; $g\,m^{-2}$)	P5	AIRS	2.3	2.82	0.99	W, W, —
	C5	AIRS	0.4	1.66	0.99	
	P5	AMSR-E	0.3	2.66	0.99	I, W, —
	C5	AMSR-E	−1.6	2.58	0.99	

CloudSat–CALIPSO, AIRS, and AMSR-E, with a particular focus on the southern midlatitudes (SMLs). Based on multiyear comparisons of P5 and C5 versions of the GISS-E2 GCM against observations, the following conclusions have been made:

1) While P5 and C5 global mean total column cloud fractions (CFs) remain within 1% of each other, the P5 total column CFs have better regional agreement with CERES-MODIS (CM) and *CloudSat–CALIPSO* (CC) retrieved CFs compared to its C5 predecessor. Changes to the PBL scheme implemented in the P5 GISS GCM have resulted in improved total column CFs, particularly in the SMLs where low-level CFs have increased by nearly 20% in relation to C5 simulations. Over the tropics, the P5-simulated total column CFs are slightly lower than the C5 results, primarily resulting from the boundary layer changes as well.
2) Although the overall global distributions of CWP from both P5 and C5 are fairly similar to CM and CS results, their global mean CWPs are higher than both CM and CS, primarily as a result of the oversimulation of CWPs within the tropics. P5-simulated CWPs over the tropics are, however, much lower than C5 results, bringing the simulation closer to observations. This improvement directly reflects the shallower boundary layer in P5. Over the tropics, the decrease in CWP from the C5 to the P5 version of the model is consistent with the decrease observed in total column CF, whereas comparing CWP and total column CF over the SMLs shows the opposite relationship, most likely an artifact attributable to a shift from stratiform cloud to shallow convection, whose condensate is not accounted for in the CWP diagnostic.
3) Precipitable water vapor comparisons show an increase in P5 simulated PWV compared to the C5 simulation, resulting from stronger convective rain evaporation in the P5 version of the GISS-E2. Compared to AIRS, the P5 results predominantly show a small positive bias throughout the model. This result is reasonable given the dry bias associated with AIRS

TABLE 2. As in Table 1, but over the SML region.

Variable	Model	Observation	Bias	RMSE	Correlation	Quicklook
CF (total; %)	P5	CM	−7.6	9.01	0.90	I, I, I
	C5	CM	−19.1	20.45	0.74	
	P5	CC	−13.7	14.37	0.90	I, I, I
	C5	CC	−25.2	26.08	0.75	
CF (high; %)	P5	CM	4.2	5.82	0.75	W, W, I
	C5	CM	−1.7	4.31	0.64	
	P5	CC	−1.9	4.84	0.68	I, I, I
	C5	CC	−7.8	9.05	0.67	
CF (mid; %)	P5	CM	9.4	10.39	0.82	W, W, I
	C5	CM	3.1	6.8	0.71	
	P5	CC	−5.1	6.78	0.92	I, I, I
	C5	CC	−11.4	13.48	0.84	
CF (low; %)	P5	CM	17.9	24.42	0.53	I, W, I
	C5	CM	−20.2	21.99	0.24	
	P5	CC	7.5	12.14	0.87	I, I, I
	C5	CC	−30.6	32.04	0.70	
CWP ($g\,m^{-2}$)	P5	CM	−19.5	68.62	0.43	W, I, I
	C5	CM	2.2	68.99	0.36	
	P5	CS	6.3	45.96	0.51	I, I, I
	C5	CS	28.0	60.84	0.34	
LWP ($g\,m^{-2}$)	P5	CS	−3.9	26.4	0.53	I, I, I
	C5	CS	21.1	49.61	0.12	
IWP ($g\,m^{-2}$)	P5	CS	10.2	50.38	0.08	W, W, W
	C5	CS	6.8	49.87	0.04	
PWV (all; $g\,m^{-2}$)	P5	AIRS	1.3	1.66	0.98	W, W, —
	C5	AIRS	0.0	0.97	0.98	
PWV (ocean; $g\,m^{-2}$)	P5	AIRS	1.3	1.67	0.98	W, W, —
	C5	AIRS	0.1	0.87	0.98	
	P5	AMSR-E	−0.6	1.07	0.99	I, I, —
	C5	AMSR-E	−1.8	1.92	0.99	

retrieval limitations in vertical range and for overcast conditions. Although the global AIRS and C5 PWV patterns and means are very close to each other, the C5-simulated PWV values are much lower than the AIRS retrievals over land. These discrepancies are reduced significantly in P5 simulations. Over the ocean, the P5 results agree better with AMSR-E retrievals globally, particularly over the SMLs.

4) The P5-simulated RHs are greater than the C5 means. For regional comparisons, both the P5 and C5 low-level RH patterns are wetter than the AIRS retrievals over the tropics, slightly more so for the P5 simulation compared to C5 results. Over the SML, the P5 and C5 low-level RHs are about 10% higher and lower than the AIRS retrievals, respectively. This finding is consistent with the CF comparison and provides strong support for the increase in the number of low-level clouds simulated by P5 over the SMLs. Over the polar regions, the GCM simulations are drier than the AIRS retrievals.
5) Spatial variability analyses using Taylor diagrams indicate overall better correlations and small standard deviations in PWV and RH comparisons between P5/C5 simulations and AMSR-E/AIRS observations. For CF and CWP/LWP/IWP comparisons, the P5 and C5 simulations have moderate correlations (~0.5–0.8) but large standard deviations (1–2σ) compared to CC results, while having low correlations (0.2–0.6) and standard deviations (~1σ) compared to CM observations. Although some improvements have been made to the P5 simulation on a global scale, large improvements have been found within the SML region, where correlations have increased while observational comparisons of bias and RMSE have significantly decreased compared to the C5 simulation.

Overall, the changes implemented in the latest P5 GISS GCM, especially the changes in boundary layer depth, have shown a significant improvement in model-simulated clouds and cloud properties. GISS GCM simulations are generating more clouds within the SML, and are beginning to produce more marine stratocumulus clouds as well. Water path and PWV measurements continue to show improvement, particularly over the SMLs. A future study will assess the TOA radiative energy budgets of the latest P5 simulations using the

TOA and surface Energy Balanced and Filled (EBAF) radiation product (Loeb et al. 2009) produced by the CERES Science team. At the time of this study, available observations contain relatively large uncertainties over polar regions. Therefore, further work will be done examining polar CFs and cloud properties once CERES edition 4 results are made publically available.

Acknowledgments. This work is supported by NASA EPSCoR CAN under Grant NNX11AM15A, NASA CERES project under Grant NNX10AI05G at the University of North Dakota, and by the NASA *CloudSat*/*CALIPSO* and Modeling and Analysis Program (MAP) RTOPs at NASA GISS, and NASA ROSES12 MAP grant to the Jet Propulsion Laboratory (JPL). NASA GISS-E2 Post-CMIP5 GCM diagnostic run data are provided by NASA GISS directly. NASA GISS E2 CMIP5 GCM data are provided by NASA GISS through the CMIP5 ESGF PCMDI database at http://pcmdi9.llnl.gov/esgf-web-fe/. The simulations were performed at the NASA Center for Climate Simulation at the Goddard Space Flight Center. CERES-MODIS *Terra* and *Aqua* SYN1deg Ed3A products used in this study are produced by the NASA CERES Team, available at http://ceres.larc.nasa.gov. *CloudSat*/*CALIPSO* 2B-CWC-RO cloud fraction data were provided by NASA CERES CCCM (Kato et al. 2010), while water path data were provided directly by JPL. AIRS V5 AIRX3STM data products are provided by NASA Goddard Earth Sciences Data and Information Services Center (GES DISC) using the Mirador data archive, available at http://mirador.gsfc.nasa.gov. AIRS V6 data were provided by JPL directly. AMSR-E data are produced by Remote Sensing Systems and sponsored by the NASA Earth Science MEaSUREs DISCOVER Project and the AMSR-E Science Team. Data are available at www.remss.com. Coauthor JHJ acknowledges the support of the NASA NDOA program, as well as that of the Jet Propulsion Laboratory, California Institute of Technology, under contract by NASA.

REFERENCES

Austin, R. T., A. J. Heymsfield, and G. Stephens, 2009: Retrieval of ice cloud microphysical parameters using the *CloudSat* millimeter-wave radar and temperature. *J. Geophys. Res.,* **114,** D00A23, doi:10.1029/2008JD010049.

Bony, S., and Coauthors, 2006: How well do we understand and evaluate climate change feedback processes? *J. Climate,* **19,** 3445–3482, doi:10.1175/JCLI3819.1.

Cess, R. D., and Coauthors, 1989: Interpretation of cloud–climate feedback as produced by 14 atmospheric general circulation models. *Science,* **245,** 513–516, doi:10.1126/science.245.4917.513.

Chiriaco, M., and Coauthors, 2007: Comparison of *CALIPSO*-like, LaRC, and MODIS retrievals of ice-cloud properties over SIRTA in France and Florida during CRYSTAL-FACE. *J. Appl. Meteor. Climatol.,* **46,** 249–272, doi:10.1175/JAM2435.1.

Collins, M., B. B. B. Booth, B. Bhaskaran, G. R. Harris, J. M. Murphy, D. M. H. Sexton, and M. J. Webb, 2011: Climate model errors, feedbacks and forcings: A comparison of perturbed physics and multi-model ensembles. *Climate Dyn.,* **36,** 1737–1766, doi:10.1007/s00382-010-0808-0.

Del Genio, A. D., Y.-H. Chen, D. Kim, and M.-S. Yao, 2012: The MJO transition from shallow to deep convection in *CloudSat*/*CALIPSO* data and GISS GCM simulations. *J. Climate,* **25,** 3755–3770, doi:10.1175/JCLI-D-11-00384.1.

Dolinar, E. K., X. Dong, B. Xi, J. H. Jiang, and H. Su, 2014: Evaluation of CMIP5 simulated clouds and TOA radiation budgets using NASA satellite observations. *Climate Dyn.,* in press.

Dong, X., P. Minnis, B. Xi, S. Sun-Mack, and Y. Chen, 2008: Comparison of CERES-MODIS stratus cloud properties with ground-based measurements at the DOE ARM Southern Great Plains site. *J. Geophys. Res.,* **113,** D03204, doi:10.1029/2007JD008438.

Fetzer, E. J., B. H. Lambrigtsen, A. Eldering, H. H. Aumann, and M. T. Chahine, 2006: Biases in total precipitable water vapor climatologies from Atmospheric Infrared Sounder and Advanced Microwave Scanning Radiometer. *J. Geophys. Res.,* **111,** D09S16, doi:10.1029/2005JD006598.

Hogan, R. J., and A. J. Illingworth, 2000: Deriving cloud overlap statistics from radar. *Quart. J. Roy. Meteor. Soc.,* **126,** 2903–2909, doi:10.1002/qj.49712656914.

Houghton, J. T., Y. Ding, D. J. Griggs, M. Noguer, P. J. van der Linden, X. Dai, K. Maskell, and C. A. Johnson, 2001: *Climate Change 2001: The Scientific Basis.* Cambridge University Press, 881 pp.

Hwang, Y., and D. M. W. Frierson, 2013: Link between the double-intertropical convergence zone problem and cloud biases over the Southern Ocean. *Proc. Natl. Acad. Sci. USA,* **110,** 4935–4940, doi:10.1073/pnas.1213302110.

Jiang, J. H., and Coauthors, 2012: Evaluation of cloud and water vapor simulations in CMIP5 climate models using NASA ''A-Train'' satellite observations. *J. Geophys. Res.,* **117,** D14105, doi:10.1029/2011JD017237.

Kato, S., S. Sun-Mack, W. F. Miller, F. G. Rose, Y. Chen, P. Minnis, and B. A. Wielicki, 2010: Relationships among cloud occurrence frequency, overlap, and effective thickness derived from *CALIPSO* and *CloudSat* merged cloud vertical profiles. *J. Geophys. Res.,* **115,** D00H28, doi:10.1029/2009JD012277.

Kennedy, A. D., X. Dong, B. Xi, P. Minnis, A. D. Del Genio, A. B. Wolf, and M. M. Khaiyer, 2010: Evaluation of the NASA GISS single-column model simulated clouds using combined surface and satellite observations. *J. Climate,* **23,** 5175–5192, doi:10.1175/2010JCLI3353.1.

Kim, D., A. H. Sobel, A. D. Del Genio, Y. Chen, S. J. Camargo, M.-S. Yao, M. Kelley, and L. Nazarenko, 2012: The tropical subseasonal variability simulated in the NASA GISS general circulation model. *J. Climate,* **25,** 4641–4659, doi:10.1175/JCLI-D-11-00447.1.

Klein, S. A., Y. Zhang, M. D. Zelinka, R. Pincus, J. Boyle, and P. J. Gleckler, 2013: Are climate model simulations of clouds improving? An evaluation using the ISCCP simulator. *J. Geophys. Res. Atmos.,* **118,** 1329–1342, doi:10.1002/jgrd.50141.

Klocke, D., R. Pincus, and J. Quaas, 2011: On constraining estimates of climate sensitivity with present-day observations

through model weighting. *J. Climate,* **24,** 6092–6099, doi:10.1175/2011JCLI4193.1.

Loeb, N. G., B. A. Wielicki, D. R. Doelling, G. L. Smith, D. F. Keyes, S. Kato, N. Manalo-Smith, and T. Wong, 2009: Toward optimal closure of the Earth's top-of-atmosphere radiation budget. *J. Climate,* **22,** 748–766, doi:10.1175/2008JCLI2637.1.

Mace, G. G., Y. Zhang, S. Platnick, M. D. King, P. Minnis, and P. Yang, 2005: Evaluation of cirrus cloud properties from MODIS radiances using cloud properties derived from ground-based data collected at the ARM SGP site. *J. Appl. Meteor.,* **44,** 221–240, doi:10.1175/JAM2193.1.

Marchand, R., G. G. Mace, T. Ackerman, and G. Stephens, 2008: Hydrometeor detection using *CloudSat*—An Earth-orbiting 94-GHz cloud radar. *J. Atmos. Oceanic Technol.,* **25,** 519–533, doi:10.1175/2007JTECHA1006.1.

Minnis, P., J. Huang, B. Lin, Y. Yi, R. F. Arduini, T.-F. Fan, J. K. Ayers, and G. G. Mace, 2007: Ice cloud properties in ice-over-water cloud systems using Tropical Rainfall Measuring Mission (TRMM) visible and infrared scanner and TRMM Microwave Imager data. *J. Geophys. Res.,* **112,** D06206, doi:10.1029/2006JD007626.

——, and Coauthors, 2008: Cloud detection in nonpolar regions for CERES using TRMM VIRS and *Terra* and *Aqua* MODIS data. *IEEE Trans. Geosci. Remote Sens.,* **46,** 3857–3884, doi:10.1109/TGRS.2008.2001351.

——, and Coauthors, 2011a: CERES edition-2 cloud property retrievals using TRMM VIRS and *Terra* and *Aqua* MODIS data—Part I: Algorithms. *IEEE Trans. Geosci. Remote Sens.,* **49,** 4374–4400, doi:10.1109/TGRS.2011.2144601.

——, and Coauthors, 2011b: CERES edition-2 cloud property retrievals using TRMM VIRS and *Terra* and *Aqua* MODIS data—Part II: Examples of average results and comparisons with other data. *IEEE Trans. Geosci. Remote Sens.,* **49,** 4401–4430, doi:10.1109/TGRS.2011.2144602.

Murphy, D. M., and T. Koop, 2005: Review of the vapour pressures of ice and supercooled water for atmospheric applications. *Quart. J. Roy. Meteor. Soc.,* **131,** 1539–1565, doi:10.1256/qj.04.94.

Naud, C. M., A. D. Del Genio, M. Bauer, and W. Kovari, 2010: Cloud vertical distribution across warm and cold in *CloudSat–CALIPSO* data and a general circulation model. *J. Climate,* **23,** 3397–3415, doi:10.1175/2010JCLI3282.1.

Olsen, E. T., and Coauthors, 2007a: AIRS/AMSU/HSB version 5 data disclaimer. Jet Propulsion Laboratory Rep., 21 pp. [Available online at http://disc.gsfc.nasa.gov/AIRS/documentation/v5_docs/AIRS_V5_Release_User_Docs/V5_Data_Disclaimer.pdf.]

——, and Coauthors, 2007b: AIRS/AMSU/HSB version 5 changes from version 4. Jet Propulsion Laboratory Rep., 22 pp. [Available online at http://disc.sci.gsfc.nasa.gov/AIRS/documentation/v5_docs/AIRS_V5_Release_User_Docs/V5_Changes_from_V4.pdf.]

——, S. Granger, E. Manning, and J. Blaisdell, 2007c: AIRS/AMSU/HSB version 5 level 3 Quick Start. Jet Propulsion Laboratory Rep., 25 pp. [Available online at http://disc.sci.gsfc.nasa.gov/AIRS/documentation/v5_docs/AIRS_V5_Release_User_Docs/V5_L3_QuickStart.pdf.]

——, and Coauthors, 2013: AIRS/AMSU/HSB version 6 changes from version 5. Jet Propulsion Laboratory Rep., 25 pp. [Available online at http://disc.sci.gsfc.nasa.gov/AIRS/documentation/v6_docs/v6releasedocs-1/V6_Changes_from_V5.pdf.]

Pincus, R., C. P. Batstone, R. J. P. Hoffman, K. E. Taylor, and P. J. Gleckler, 2008: Evaluating the present-day simulation of clouds, precipitation, and radiation in climate models. *J. Geophys. Res.,* **113,** D14209, doi:10.1029/2007JD009334.

Platnick, S., M. D. King, S. A. Ackerman, W. P. Menzel, B. A. Baum, J. C. Riedi, and R. A. Frey, 2003: The MODIS cloud products: Algorithms and examples from *Terra*. *IEEE Trans. Geosci. Remote Sens.,* **41** (2), 459–473, doi:10.1109/TGRS.2002.808301.

Randall, D. A., and Coauthors, 2007: Climate models and their evaluation. *Climate Change 2007: The Physical Science Basis,* S. Solomon et al., Eds., Cambridge University Press, 589–662.

Rossow, W. B., and R. A. Schiffer, 1999: Advances in understanding clouds from ISCCP. *Bull. Amer. Meteor. Soc.,* **80,** 2261–2287, doi:10.1175/1520-0477(1999)080<2261:AIUCFI>2.0.CO;2.

Schmidt, G. A., and Coauthors, 2006: Present-day atmospheric simulations using GISS ModelE: Comparison to in situ, satellite, and reanalysis data. *J. Climate,* **19,** 153–192, doi:10.1175/JCLI3612.1.

——, and Coauthors, 2014: Configuration and assessment of the GISS ModelE2 contributions to the CMIP5 archive. *J. Adv. Model. Earth Syst.,* **6,** 141–184, doi:10.1002/2013MS000265.

Stanfield, R., 2012: Assessment of NASA GISS CMIP5 ModelE simulated clouds and TOA radiation budgets using satellite observations over the southern mid-latitudes. Master's thesis, Department of Atmospheric Sciences, University of North Dakota, 86 pp.

Stephens, G. L., 2005: Cloud feedbacks in the climate system: A critical review. *J. Climate,* **18,** 237–273, doi:10.1175/JCLI-3243.1.

——, and Coauthors, 2002: The *CloudSat* mission and the A-Train. *Bull. Amer. Meteor. Soc.,* **83,** 1771–1790, doi:10.1175/BAMS-83-12-1771.

Stubenrauch, C. J., and Coauthors, 2013: Assessment of global cloud datasets from satellites: Project and database initiated by the GEWEX Radiation Panel. *Bull. Amer. Meteor. Soc.,* **94,** 1031–1049, doi:10.1175/BAMS-D-12-00117.1.

Taylor, K. E., 2001: Summarizing multiple aspects of model performance in a single diagram. *J. Geophys. Res.,* **106,** 7183–7192, doi:10.1029/2000JD900719.

——, R. J. Stouffer, and G. A. Meehl, 2012: An overview of CMIP5 and the experiment design. *Bull. Amer. Meteor. Soc.,* **93,** 485–498, doi:10.1175/BAMS-D-11-00094.1.

Trenberth, K. E., and J. T. Fasullo, 2010: Simulation of present-day and twenty-first-century energy budgets of the southern oceans. *J. Climate,* **23,** 440–454, doi:10.1175/2009JCLI3152.1.

Waliser, D., and Coauthors, 2009: Cloud ice: A climate model challenge with signs and expectations of progress. *J. Geophys. Res.,* **114,** D00A21, doi:10.1029/2008JD010015.

Wentz, F. J., 1997: A well-calibrated ocean algorithm for Special Sensor Microwave/Imager. *J. Geophys. Res.,* **102,** 8703–8718, doi:10.1029/96JC01751.

Wielicki, B. A., R. D. Cess, M. D. King, D. A. Randall, and E. F. Harrison, 1995: Mission to planet Earth: Role of clouds and radiation in climate. *Bull. Amer. Meteor. Soc.,* **76,** 2125–2153, doi:10.1175/1520-0477(1995)076<2125:MTPERO>2.0.CO;2.

——, B. R. Barkstrom, E. F. Harrison, R. B. Lee III, G. L. Smith, and J. E. Cooper, 1996: Clouds and the Earth's Radiant Energy System (CERES): An Earth Observing System Experiment. *Bull. Amer. Meteor. Soc.,* **77,** 853–868, doi:10.1175/1520-0477(1996)077<0853:CATERE>2.0.CO;2.

Winker, D. M., W. H. Hunt, and M. J. McGill, 2007: Initial performance assessment of CALIOP. *Geophys. Res. Lett.,* **34,** L19803, doi:10.1029/2007GL030135.

Xi, B., X. Dong, P. Minnis, and M. M. Khaiyer, 2010: A 10-year climatology of cloud cover and vertical distribution derived from both surface and GOES observations over the DOE ARM SGP site. *J. Geophys. Res.,* **115,** D12124, doi:10.1029/2009JD012800.

Yao, M.-S., and Y. Cheng, 2012: Cloud simulations in response to turbulence parameterizations in the GISS Model E GCM. *J. Climate,* **25,** 4963–4974, doi:10.1175/JCLI-D-11-00399.1.

Yoo, H., and Z. Li, 2012: Evaluation of cloud properties in the NOAA/NCEP global forecast system using multiple satellite products. *Climate Dyn.,* **39,** 2769–2787, doi:10.1007/s00382-012-1430-0.

——, ——, Y.-T. Hou, S. Lord, F. Weng, and H. W. Barker, 2013: Diagnosis and testing of low-level cloud parameterizations for the NCEP/GFS using satellite and ground-based measurements. *Climate Dyn.,* **41,** 1595–1613, doi:10.1007/s00382-013-1884-8.

Zhang, M. H., and Coauthors, 2005: Comparing clouds and their seasonal variations in 10 atmospheric general circulation models with satellite measurements. *J. Geophys. Res.,* **110,** D15S02, doi:10.1029/2004JD005021.